Langmuir
Article
pubs.acs.org/Langmuir

One-Phase Synthesis of Water-Soluble Gold Nanoparticles with Control over Size and Surface Functionalities

Eunkeu Oh,[†] Kimihiro Susumu,[†] Ramasis Goswami,[‡] and Hedi Mattoussi*[,†,§]

[†]*Division of Optical Sciences, Code 5611 and* [‡]*Materials Science Division, Code 6355, U.S. Naval Research Laboratory, Washington, D.C. 20375.* [§]*Present address: Department of Chemistry and Biochemistry, Florida State University, 4006 Chemical Sciences Building, Tallahassee, Florida 32306.*

Received November 23, 2009. Revised Manuscript Received January 7, 2010

We report a simple and efficient synthetic method to prepare gold nanoparticles (AuNPs) in aqueous phase using $HAuCl_4$ and poly(ethylene glycol) (PEG) ligands appended with bidentate anchoring groups. Our approach provides narrow size distribution nanocrystals over the size range between 1.5 and 18 nm; this range is much wider than those achieved using other small molecules and polymer ligands. The NP size was simply controlled by varying the molar ratio of Au-to-PEG ligand precursors. Further passivation of the as-prepared AuNPs permitted *in situ* functionalization of the NP surface with the desired functional groups. The prepared AuNPs exhibit remarkable stability in the presence of high salt concentrations, over a wide range of pHs (2−13), and a strong resistance to competition from dithiothreitol (DTT). These results are a clear manifestation of the advantages offered by our synthetic approach to prepare biocompatible AuNPs, where modular, multifunctional ligands presenting strong anchoring groups and hydrophilic PEG chains are used.

Introduction

Gold nanoparticles (AuNPs) along with an array of other metallic and semiconducting nanocrystals with their size-dependent physical and chemical properties have generated a tremendous interest in the past decade. This interest has also been driven by the great potential for applications in optical and electronic devices and more recently in biological sensing and imaging.[1−3] AuNPs with size larger than 2 nm (in diameter) exhibit size- and shape-dependent surface plasmon absorption band (SPB); AuNPs smaller than 2 nm, in comparison, exhibit photoinduced emission.[4] The SPB is also sensitive to proximity-driven NP-to-NP interactions and to the surrounding environment, including surface ligands, solvent, and temperature. Thus, red shift of the SPB coupled with broadening of the peak width has been observed in the presence of NP aggregation, which can be triggered by interactions with a particular target or in response to an external stimulus (changes in pH or excess ion concentrations). Larger size AuNPs and nanorods can also transform laser excitation to local thermal heating. These unique properties have provided researchers in biology with powerful methods to develop sensing techniques that include (1) colorimetric assays to detect NP assemblies,[1,5,6] (2) molecular rulers based on plasmon coupling to detect bridging between NP pairs (e.g., DNA hybridization),[7,8] (3) surface-enhanced Raman scattering (SERS) nanoparticle tags for *in vivo* spectroscopy,[9,10] and (4) photoinduced heating of Au nanoparticles and nanorods for localized photothermal therapy.[11,12] Recently, the size-dependent uptake of AuNPs by live cells was studied for sizes ranging from 2 to 100 nm.[13−15] AuNPs are also efficient quenchers of dyes and luminescent quantum dots (via resonance energy transfer) when brought in close proximity.[16,17] These applications often require that the AuNPs are (1) available in a broad size range, (2) stable over a broad range of conditions, and (3) easy to surface functionalize with specific reactive groups for further coupling to target molecules.

Since the classic citrate reduction of aurate to prepare citrate-stabilized AuNPs was pioneered by the groups of Turkevich and Frens,[18,19] there has been a sustained effort aimed at developing new chemical routes to prepare AuNPs that are stable and easily dispersible in water. These efforts have also focused on designing synthetic schemes to functionalize the AuNP surfaces with specific target ligands.[20] Some of the most common methods

*To whom correspondence should be addressed. E-mail: mattoussi@chem.fsu.edu.

(1) Daniel, M. C.; Astruc, D. *Chem. Rev*. **2004**, *104*, 293–346.
(2) Zheng, J.; Nicovich, P. R.; Dickson, R. M. *Annu. Rev. Phys. Chem*. **2007**, *58*, 409–431.
(3) De, M.; Ghosh, P. S.; Rotello, V. M. *Adv. Mater*. **2008**, *20*, 4225–4241.
(4) Schaeffer, N.; Tan, B.; Dickinson, C.; Rosseinsky, M. J.; Laromaine, A.; McComb, D. W.; Stevens, M. M.; Wang, Y. Q.; Petit, L.; Barentin, C.; Spiller, D. G.; Cooper, A. I.; Levy, R. *Chem. Commun*. **2008**, 3986–3988.
(5) Mirkin, C. A.; Letsinger, R. L.; Mucic, R. C.; Storhoff, J. J. *Nature* **1996**, *382*, 607–609.
(6) Lee, J. S.; Ulmann, P. A.; Han, M. S.; Mirkin, C. A. *Nano Lett*. **2008**, *8*, 529–533.
(7) Sonnichsen, C.; Reinhard, B. M.; Liphardt, J.; Alivisatos, A. P. *Nat. Biotechnol*. **2005**, *23*, 741–745.
(8) Reinhard, B. M.; Siu, M.; Agarwal, H.; Alivisatos, A. P.; Liphardt, J. *Nano Lett*. **2005**, *5*, 2246–2252.
(9) Qian, X. M.; Peng, X. H.; Ansari, D. O.; Yin-Goen, Q.; Chen, G. Z.; Shin, D. M.; Yang, L.; Young, A. N.; Wang, M. D.; Nie, S. M. *Nat. Biotechnol*. **2008**, *26*, 83–90.
(10) Qian, X. M.; Nie, S. M. *Chem. Soc. Rev*. **2008**, *37*, 912–920.
(11) Huang, X. H.; Jain, P. K.; El-Sayed, I. H.; El-Sayed, M. A. *Lasers Med. Sci*. **2008**, *23*, 217–228.
(12) Jain, P. K.; Huang, X. H.; El-Sayed, I. H.; El-Sayed, M. A. *Acc. Chem. Res*. **2008**, *41*, 1578–1586.
(13) Jiang, W.; Kim, B. Y. S.; Rutka, J. T.; Chan, W. C. W. *Nat. Nanotechnol*. **2008**, *3*, 145–150.
(14) Wang, S. G.; Lu, W. T.; Tovmachenko, O.; Rai, U. S.; Yu, H. T.; Ray, P. C. *Chem. Phys. Lett*. **2008**, *463*, 145–149.
(15) Perrault, S. D.; Walkey, C.; Jennings, T.; Fischer, H. C.; Chan, W. C. W. *Nano Lett*. **2009**, *9*, 1909–1915.
(16) Dulkeith, E.; Morteani, A. C.; Niedereichholz, T.; Klar, T. A.; Feldmann, J.; Levi, S. A.; van Veggel, F. C. J. M.; Reinhoudt, D. N.; Moller, M.; Gittins, D. I. *Phys. Rev. Lett*. **2002**, *89*, 203002.
(17) Oh, E.; Hong, M. Y.; Lee, D.; Nam, S. H.; Yoon, H. C.; Kim, H. S. *J. Am. Chem. Soc*. **2005**, *127*, 3270–3271.
(18) Turkevich, J.; Stevenson, P. C.; Hillier, J. *Discuss. Faraday Soc*. **1951**, 55–.
(19) Frens, G. *Nat. Phys*. **1973**, *241*, 20–22.
(20) Weisbecker, C. S.; Merritt, M. V.; Whitesides, G. M. *Langmuir* **1996**, *12*, 3763–3772.

include the following: (1) Growth of 1.5−5.2 nm AuNPs surface-functionalized with alkanethiol using two-phase toluene/water reaction developed by Brust and co-workers;[21,22] this route produced hydrophobic nanoparticles. (2) Use of poly(ethylene glycol) oligomer (PEG) containing ligands combined with the two-phase reaction developed by Brust and co-workers, to prepare Au clusters first reported by Murray et al.[23] and then later by Brust et al.[24] The resulting NPs (water dispersible) are capped with either monothiol-terminated PEG (MW 5000) oligomers,[23] or tetraethylene glycol ligands.[24] (3) Use of dialkyl disulfide stabilizers to prepare 1.4−3.8 nm diameter AuNPs.[25,26] (4) Synthesis of 1.5−8 nm size of AuNPs using water-soluble alkyl thioether- and thiol-functionalized poly(methacrylic acid).[27,28] (5) Preparation of phosphine-stabilized 1.4 nm AuNPs;[29] 1.4 nm AuNPs surface-functionalized with maleimide are commercially available (Nanoprobes, Yaphank, NY). These preparation methods reflect the tremendous progress made in the past decade. They provided researchers with an array of AuNPs which have been employed for developing a variety of applications. Nonetheless, each of these synthetic schemes has encountered some limitations. These include (1) reduced stability against excess salts and changes in solution pH (e.g., citrate-stabilized NPs); (2) the inability to prepare nanocrystals over a wide size regime (citrate reduction usually produces AuNPs smaller than 10 nm, but larger sizes require additional refluxing in the presence of sodium citrate); (3) most NPs prepared using thiol−alkyl−Au interactions are hydrophobic, and the transfer to aqueous media further requires postsynthetic processing via ligand exchange, which can be tedious and requires large amounts of ligands. Murphy and co-workers combined seeding, growth, and temperature treatment in the presence of cetyltrimethylammonium bromide (CTAB) to synthesize larger size AuNPs and Au nanorods (5−40 nm range).[30] These findings combined clearly indicate that, despite the tremendous progress, there is still a need to develop new simple synthetic methods to prepare AuNPs over a wide range of sizes that exhibit enhanced stability in buffer media (often rich in ionic complexes) and which can be surface-functionalized.

We have designed and synthesized an array of modular ligands made of a tunable length PEG segment appended with either a thioctic acid (TA, which has a terminal disulfide) or a dihydrolipoic acid (DHLA, formed by reducing the terminal disulfide to dithiol) at one end and a potentially reactive group at another end (see Figure 1).[31−34] The synthetic procedures we have developed are simple to implement and provide multigram scale of materials. We have also shown that both TA-PEG- and DHLA-PEG-based ligands can be used to cap-exchange citrate-stabilized NPs. In addition, we have demonstrated that DHLA-PEG ligands provide effective surface functionalization of semiconductor quantum dots and promote their transfer to buffer media. Furthermore, the bidentate nature of the anchoring group provides better stability to both types of nanocrystals compared with their monothiol analogues.[32,33]

Here, we build on the synthetic rationales reported for the preparation of thiol stabilized AuNPs combined with the nature of our TA-PEG ligands to develop a simple one-phase (aqueous) growth and passivation method to prepare a series of hydrophilic AuNPs. This new route provides nanocrystals with a broad range of sizes (1.5−18 nm in diameter), which can also be readily functionalized with reactive end groups for further coupling to target bioreceptors. Since these NPs are stabilized with disulfide anchoring groups, they exhibit remarkable stability in the presence of excess counterions, against competition with dithiothreitol (DTT), and to changes in solution pH, similar to what was reported for Au nanoparticles cap-exchanged with TA-PEG ligands (starting with citrate-coated NPs) or prepared in the presence of thiol-functionalized polymers.[28,35] We describe the synthetic details developed and discuss optical and structural characterization of the prepared AuNPs using UV−vis spectroscopy, high-resolution transmission electron microcopy (HRTEM), and dynamic light scattering (DLS).

Results and Discussion

Control of Au Nanocrystal Growth. For this study, we synthesized TA-PEG-OCH_3 ligands with average poly(ethylene glycol) methyl ether molecular weight (MW) of 550 or 750. Ligands with a PEG MW ~ 550 (TA-PEG550-OCH_3) were used throughout this report, unless otherwise noted. For *in situ* functionalization, we used TA-PEG600-COOH (PEG MW ~ 600) ligand mixed with TA-PEG-OCH_3 during AuNP synthesis.

Synthesis of TA-PEG-OCH_3 and TA-PEG600-COOH was carried out following the procedures detailed in our previous reports.[32−34] For control experiments, we used mercaptohexanoic-acid-appended PEG (HS-PEG550-OCH_3, monothiol appended ligand). The synthetic details are provided in the Experimental Section. The AuNPs were prepared using a three-step reaction consisting of (1) precursor formation by reacting the ligands with tetrachloroauric(III) acid ($HAuCl_4 \cdot 3H_2O$); (2) growth of the AuNP cores triggered by addition of $NaBH_4$ reducing agent; and (3) further passivation and functionalization of the cores by adding extra free ligands, as schematically diagrammed in Figure 1. Tetrachloroauric acid and the ligands were first mixed in water to promote the formation of Au-TA-PEG-OCH_3 metal−ligand precursors. This precursor formation manifests in a rapid color change of the original yellow solution to red, yellow, and finally colorless. Addition of $NaBH_4$ initiates reduction of the Au ions and rapid growth of the Au nanocrystals. We varied the molar ratio of Au-to-ligand as a means of controlling the size of the resulting metal core. Once the growth was complete (usually associated with a saturation in the UV−vis absorption spectrum), free ligands were further added to the solution (to a final Au/ligand molar ratio of ~1:1). This last step provided additional passivation and functionalization (when desired) of the AuNPs by filling unoccupied surface sites. Nonetheless, when NPs were grown under initial low Au-to-ligand

(21) Brust, M.; Walker, M.; Bethell, D.; Schiffrin, D. J.; Whyman, R. *J. Chem. Soc., Chem. Commun.* **1994**, 801–802.
(22) Brust, M.; Fink, J.; Bethell, D.; Schiffrin, D. J.; Kiely, C. *J. Chem. Soc., Chem. Commun.* **1995**, 1655–1656.
(23) Wuelfing, W. P.; Gross, S. M.; Miles, D. T.; Murray, R. W. *J. Am. Chem. Soc.* **1998**, *120*, 12696–12697.
(24) Kanaras, A. G.; Kamounah, F. S.; Schaumburg, K.; Kiely, C. J.; Brust, M. *Chem. Commun.* **2002**, 2294–2295.
(25) Yonezawa, T.; Yasui, K.; Kimizuka, N. *Langmuir* **2001**, *17*, 271–273.
(26) Shon, Y. S.; Mazzitelli, C.; Murray, R. W. *Langmuir* **2001**, *17*, 7735–7741.
(27) Hussain, I.; Graham, S.; Wang, Z. X.; Tan, B.; Sherrington, D. C.; Rannard, S. P.; Cooper, A. I.; Brust, M. *J. Am. Chem. Soc.* **2005**, *127*, 16398–16399.
(28) Wang, Z. X.; Tan, B. E.; Hussain, I.; Schaeffer, N.; Wyatt, M. F.; Brust, M.; Cooper, A. I. *Langmuir* **2007**, *23*, 885–895.
(29) Weare, W. W.; Reed, S. M.; Warner, M. G.; Hutchison, J. E. *J. Am. Chem. Soc.* **2000**, *122*, 12890–12891.
(30) Jana, N. R.; Gearheart, L.; Murphy, C. J. *Langmuir* **2001**, *17*, 6782–6786.
(31) Uyeda, H. T.; Medintz, I. L.; Jaiswal, J. K.; Simon, S. M.; Mattoussi, H. *J. Am. Chem. Soc.* **2005**, *127*, 3870–3878.
(32) Susumu, K.; Uyeda, H. T.; Medintz, I. L.; Pons, T.; Delehanty, J. B.; Mattoussi, H. *J. Am. Chem. Soc.* **2007**, *129*, 13987–13996.
(33) Mei, B. C.; Susumu, K.; Medintz, I. L.; Delehanty, J. B.; Mountziaris, T. J.; Mattoussi, H. *J. Mater. Chem.* **2008**, *18*, 4949–4958.
(34) Susumu, K.; Mei, B. C.; Mattoussi, H. *Nat. Protoc.* **2009**, *4*, 424–436.
(35) Mei, B. C.; Oh, E.; Susumu, K.; Farrell, D.; Mountziaris, T. J.; Mattoussi, H. *Langmuir* **2009**, *25*, 10604–10611.

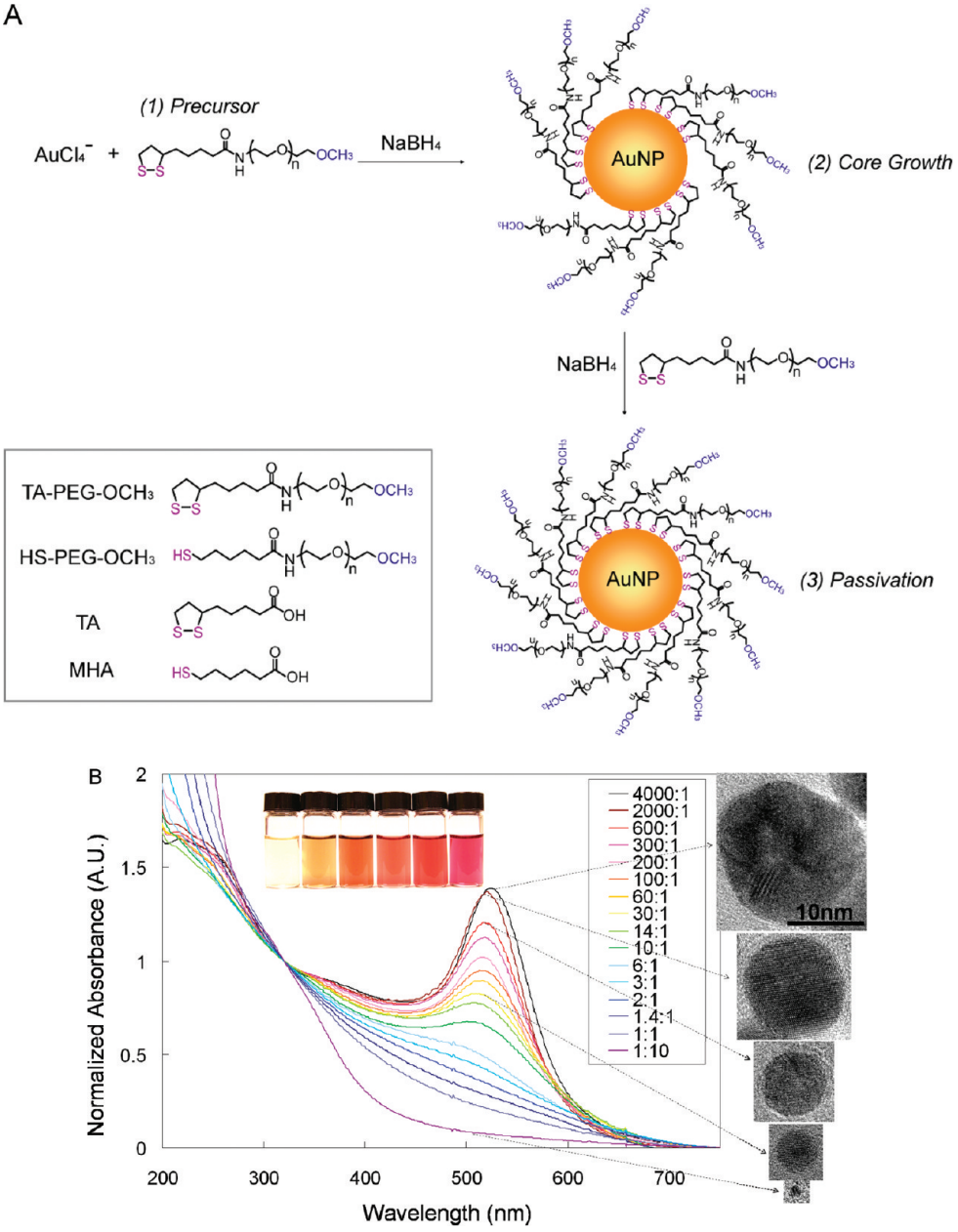

Figure 1. (A) Schematic representation of the one-phase growth method using TA-PEG-OCH_3 ligands. (B) Normalized UV−vis absorption spectra for several Au/ligand molar ratios used for the growth (of AuNPs with different sizes), along with a few representative TEM images collected for selected subsets of these nanocrystals. (inset) Image collected from a series of AuNP dispersions in deionized water. Changes in solution color from light to dark brown and to red (from left to right) reflect increase in AuNP size.

molar ratio (smaller than 1:1), no extra free ligands were added to the final sample; the initial molar concentration of the ligands was high enough to provide sufficient passivation of the nanoparticles in this case.

In a typical reaction, the following conditions were used to prepare our AuNPs. An amount of 156 μL (7.92×10^{-6} mol) of 50.8 mM tetrachloroauric(III) acid ($HAuCl_4 \cdot 3H_2O$) stock solution and the desired molar concentration of TA-PEG550-OCH_3 were dissolved in 25 mL of deionized water; the mixture was then stirred at room temperature for 1 h. The stock solution of ($HAuCl_4 \cdot 3H_2O$) was prepared by mixing 100 mg (2.54×10^{-4} mol) of $AuCl_4$ in 5 mL of H_2O. Stirring for 1 h was based on the anticipated minimum time necessary to promote precursor formation (see below). An amount of 72 μL (6.3×10^{-5} mol) of 880 mM sodium borohydride ($NaBH_4$) stock solution in deionized water was added (in aliquots of 18 μL) over 30 min with vigorous stirring. To prepare different size nanoparticles, we fixed the molar concentration of $HAuCl_4$ and varied the amount of the ligands used. Following addition of the reducing agent, the color of the reaction mixture immediately changed to brown or red depending on size. The mixture was then left stirring for at least 3 h, as it gradually progressed to its final appearance (when the absorption spectrum reached saturation). The AuNP dispersions (as-prepared) were characterized using UV−vis spectroscopy, TEM, and DLS. For extra passivation (or passivation and functionalization), TA-PEG550-OCH_3 or a mixture of either TA-PEG550-OCH_3/TA-PEG600-COOH or TA-PEG550-OCH_3/TA-PEG600-NH_2 (final ratio of Au to ligand = 1:1) and 18 μL (1.6×10^{-5} mol) of 880 mM $NaBH_4$ were further added to the AuNP solution, and left stirring for an additional 3 h. The dispersion was then purified from free ligands by three cycles of centrifugation using a membrane filtration device (Millipore).

These AuNPs were then characterized and compared to those not subjected to the extra passivation/functionalization step. In our experimental protocol, we used 10× total molar excess of the reducing agent during the growth and passivation steps (i.e., total $NaBH_4$-to-Au molar ratio ~ 10). This value was based on those used in previous studies and provided the most effective preparation conditions including those reported using the Brust method.[21] Reducing this ratio to 9 or 8 does not change the results. Lower values (e.g., ~1×), however, do not provide growth of homogeneous AuNP dispersions. As controls, we synthesized thioctic acid (TA)−AuNPs, mercaptohexanoic acid (MHA)−AuNPs, and HS-PEG-OCH_3−AuNPs using the same method but mixing either TA, MHA, or monothiol-appended PEG ligands instead of TA-PEG-OCH_3 (Figure 1A).

Characterization of the AuNPs. *1. UV−Vis Absorption Spectroscopy*. Figure 1B shows the absorption spectra collected from a set of AuNP dispersions prepared using an increased molar ratio of Au to TA-PEG-OCH_3; some representative TEM images collected from these dispersions are also shown. The absorption spectra show that at low Au-to-ligand molar ratio the characteristic SPB located at 520 nm is very weak (not discernible for the smallest size NPs). However, the peak becomes sharper and more defined at Au/ligand molar ratios above 6:1. The well-defined and narrow SPB peaks for these dispersions (in particular for those prepared with high Au-to-ligand molar ratios) indicate that narrow size distribution characterizes these NPs. The inset shows an image of several NP dispersions in deionized water. The dispersion color changed from dark yellow to brown and then to red as the Au-to-TA-PEG-OCH_3 ligand ratio increased, indicating an increase in the NP size. Data clearly indicate that our NP growth method is capable of providing high quality nanocrystals over a broad size range, where effective control over the NP dimensions has simply been achieved by varying the Au/ligand ratio used during growth.

The growth reaction carried out in the presence of TA, MHA and HS-PEG-OCH_3 yielded only smaller size AuNPs (diameter < 10 nm). In addition, dispersions prepared using high Au/ligand ratios easily precipitated when monothiol-appended ligands were used (see Figure S1 in the Supporting Information). For instance, dynamic light scattering experiments indicated the presence of aggregate buildup (~190 nm size) for the dispersions of HS-PEG-OCH_3−AuNPs (see Figure S2 in the Supporting Information). The rest of the structural characterization will focus on nanocrystals prepared using TA-PEG-OCH_3 ligands.

2. Transmission Electron Microscopy (*TEM*). We relied on the use of high-resolution TEM to determine nanocrystal sizes and assess their crystalline quality; only data collected from TA-PEG-OCH_3−AuNPs are shown. Figure 2 shows the TEM images collected from six representative nanocrystal dispersions prepared using a Au/TA-PEG-OCH_3 ratio that varied from 1:10 to 4000:1. The images show that the size of the NPs progressively increased with increasing Au-to-ligand molar ratio, as anticipated from the absorption properties shown in Figure 1B. The average diameter extracted from these TEM images together with the Au/ligand ratios are listed in Table 1. Typically, the measured diameters were 1.5 ± 0.3 nm (for Au/ligand = 1:10), 2.2 ± 0.3 nm (for Au/ligand = 1.4:1), 4.6 ± 0.4 nm (Au/ligand = 30:1), 10 ± 1.4 nm (Au/ligand = 600:1), 12 ± 1.7 nm (Au/ligand = 2000:1), and 18 ± 3.3 nm (Au/ligand = 4000:1), respectively. These images do not show any sign of nanocrystal clumping on the TEM grid, further confirming the colloidal stability of these dispersions. The TEM images also show that spherical shapes dominate the dispersions of small size nanocrystals. However, slight inhomogeneities in nanoparticle shape are observed for the larger size NPs (see panel 6 in Figure 2A). Higher resolution images for a few representative nanocrystal sizes with different crystal orientations are shown in Figure 2B together with the corresponding fast Fourier transformation (FFT) and inversed FFT (IFFT). The lattice spacing along the (111) planes measured for our nanocrystals was 2.4 Å, in agreement with what has been previously reported (2.36 Å) for

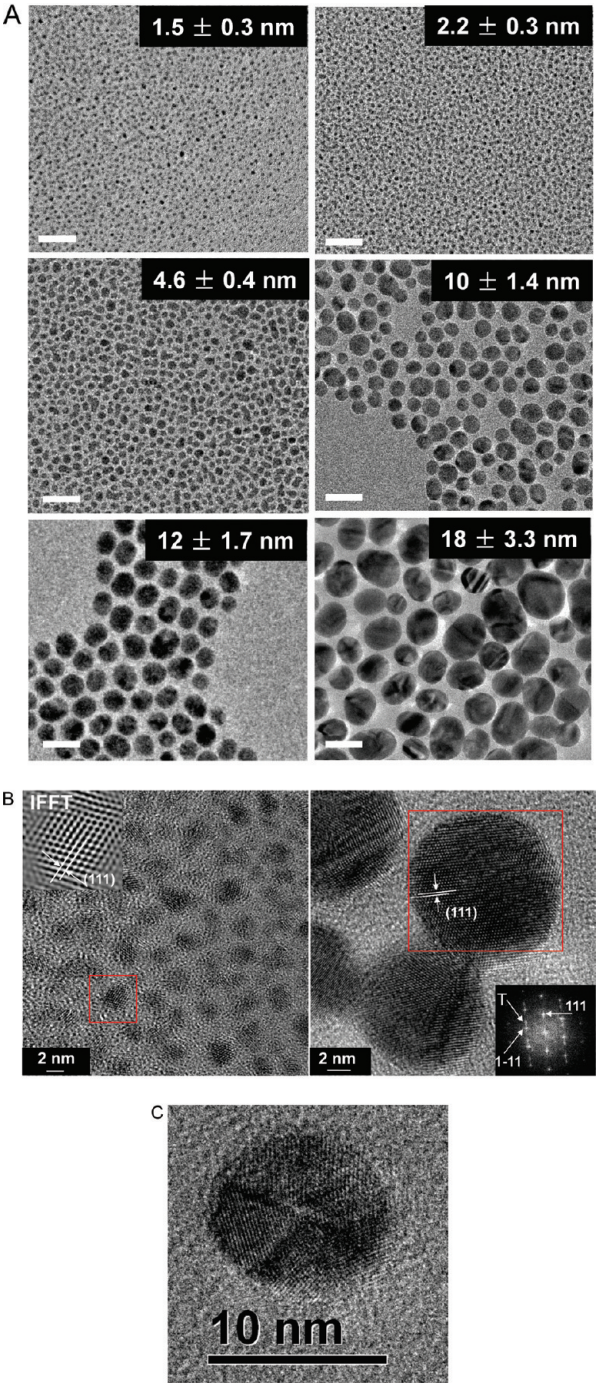

Figure 2. (A) TEM images of several different size AuNPs (scale bar = 20 nm). Average size and standard deviation are reported for each sample. Samples for TEM were prepared by spreading a drop of the AuNP dispersions onto the TEM grid (made of a holey carbon film on a 400 mesh Cu grid). (B) IFFT of the TEM image of 2.2 nm TA-PEG-OCH_3−AuNPs (inset, upper left) and FFT of 12 nm TA-PEG-OCH_3−AuNPs (inset, lower right). T indicates the twin plane in the lower right inset. Lattice spacing is about 0.24 nm for both. (C) High-resolution image of a larger size NP showing multiple twinning, which is characteristic of FCC structure.

Table 1. Sizes Extracted from High-Resolution TEM and DLS Experiments Shown Together with the Corresponding Au-to-Ligand Ratios Used throughout the Study

Au/ligand ratio[a]	TEM (nm)	DLS (nm)[b]	DLS (nm)[c]
1:10	1.5 ± 0.3		
1:1	1.7 ± 0.2		
1.4:1	2.2 ± 0.3		
3:1	2.4 ± 0.3		
10:1	3.0 ± 0.5		
20:1	4.3 ± 0.6		
30:1	4.6 ± 0.4	11 ± 2.4	13 ± 2.7
100:1	5.0 ± 0.7		
250:1	7 ± 1.2	13 ± 2.8	19 ± 4.6
300:1	8 ± 0.9		
600:1	10 ± 1.4	16 ± 3.6	21 ± 3.8
2000:1	12 ± 1.7	21 ± 4.0	25 ± 5.3
4000:1	18 ± 3.3	27 ± 8.4	33 ± 13

[a] Precursor ratios used during core synthesis of AuNPs. [b] Sizes measured for as-prepared AuNP dispersions. [c] Sizes measured after the extra passivation step with additional ligands.

face-centered cubic (FCC) AuNPs.[36] The TEM images also show that twinning defects characteristic of FCC crystalline structures are observed primarily for the larger size nanocrystals (see Figure 2C). A plot summarizing the progression of particle size (extracted from TEM) versus Au-to-ligand ratio for the full set of nanocrystals prepared using our growth method is shown in Figure 3A. To further test the quality of our AuNPs, we plotted the progression of the extinction coefficient at 520 nm versus diameter (based on TEM measurements) together with those measured for commercially available citrate-stabilized AuNPs (Ted Pella Inc.); see Figure 3B. The data are essentially identical for both sets of NPs. The overall trend for the nanocrystal size versus Au-to-ligand ratio compiled for our materials indicates a rapid size increase at low ratios (Au/ligand ≤ 10:1, diameter ≤ 3 nm). This dependence becomes moderate for the medium size range (diameter ∼ 3−10 nm, Au/ligand ratio ∼ 10−600) and eventually very weak for large size NPs (diameter > 10 nm, at Au-to-ligand ratio exceeding ∼600). The rapid size change measured at low ratios reflects the pronounced effects of surface-to-volume ratios for small size NPs; this ratio is sensitive to the amounts of ligands used. As the NP size increases and the relative surface-to-volume ratios decreases, effects of ligand concentration become less dominant, which translates into a weaker change in NP size at rather large Au/ligand ratios. We should emphasize that the size range described here is not exclusive, as slightly smaller NPs (∼1−1.4 nm) and larger size nanocrystals (∼20 nm) can be made. We were not able to collect high quality TEM images for NPs smaller than 1.5 nm, due to weaker electronic contrast and potential interference from the ligands; we also limited our characterization of the largest size to 18 nm NPs. Use of thiol-terminated poly(methacrylic acid) (as ligand) for the synthesis of water-soluble AuNPs has been reported by Brust and co-workers.[27,28] The authors also explored the effects of changing the exact polymer structure as well as hydrophobicity and/or "denticity" of the end groups on the size and distribution of prepared NPs. In particular, they showed that AuNPs with sizes ranging from 1.5 to 8 nm can be made.[28]

3. Dynamic Light Scattering (DLS). Dynamic light scattering (DLS) is a powerful technique that has widely been used to probe the stability of colloidal dispersions and polymeric solutions.[37−39] Due to the extreme sensitivity of the scattered

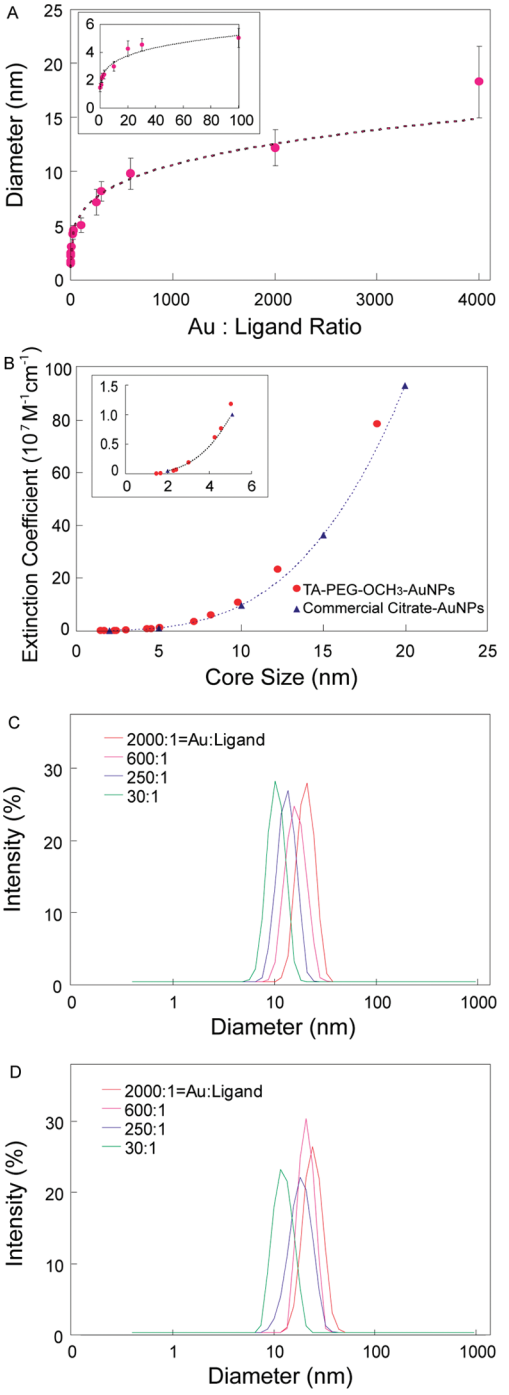

Figure 3. (A) Plot of the AuNP size measured by TEM versus Au-to-TA-PEG-OCH_3 molar ratio. Inset shows a blow up of the region near the origin (small ratios). (B) Plot of the extinction coefficients of AuNPs, calculated from UV−vis absorbance at 520 nm, versus diameter extracted from TEM. Inset shows a blow up of the section corresponding to small ratios. (C) Intensity versus hydrodynamic diameter profiles extracted from DLS for TA-PEG-OCH_3−AuNPs (as-prepared) with different Au-to-ligand molar ratios: 2000:1, 600:1, 250:1, and 30:1. The corresponding hydrodynamic diameters are 21 ± 4.0 nm, 16 ± 3.6, 13 ± 2.8, and 11 ± 2.4, respectively. (D) Intensity versus hydrodynamic diameter profiles for the same series after the extra passivation.

(36) Kuo, C. H.; Chiang, T. F.; Chen, L. J.; Huang, M. H. *Langmuir* **2004**, *20*, 7820–7824.
(37) Berne, B. J.; Pecora, R. *Dynamic light scattering: with applications to chemistry, biology, and physics*; Dover Publications: Mineola, NY, 2000.
(38) Brown, W. *Dynamic light scattering: the method and some applications*; Clarendon Press: Oxford, New York, 1993.
(39) Pons, T.; Uyeda, H. T.; Medintz, I. L.; Mattoussi, H. *J. Phys. Chem. B* **2006**, *110*, 20308–20316.

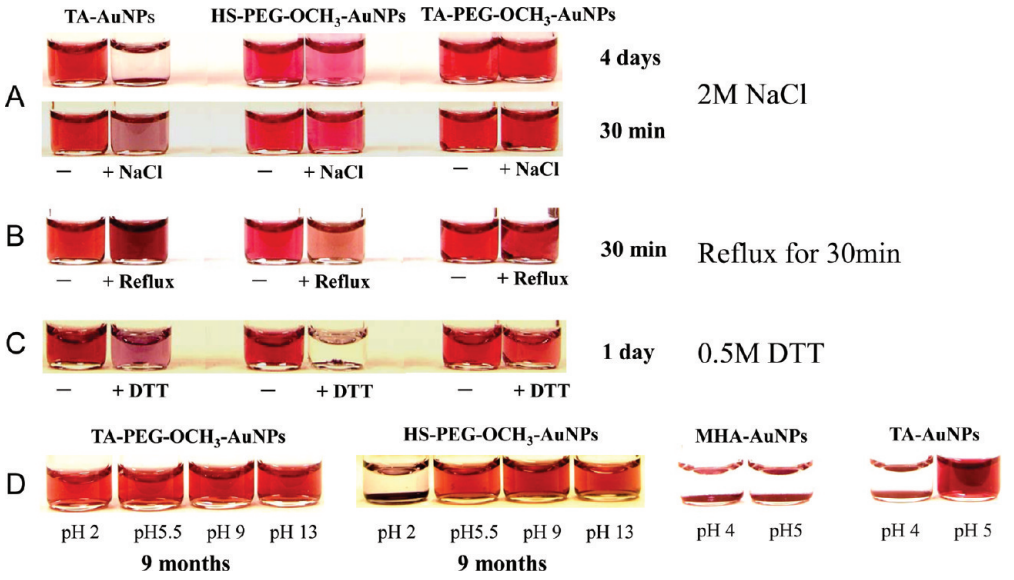

Figure 4. Images of AuNP dispersions under various conditions: (A) TA-PEG-OCH_3−AuNP dispersions without (−) and with (+) 2 M NaCl after 30 min and 4 days at room temperature; (B) images of NPs subjected to refluxing at 100 °C for 30 min; and (C) NP dispersions mixed with 0.5 M DTT at pH 8 and kept at room temperature for 1 day. (D) pH stability test of AuNPs synthesized with the various ligands after 9 months of storage at room temperature.

signal to changes in the radius (R) of the scattering objects (scattered intensity $\propto R^6$), DLS can detect even small fractions of aggregate buildup in NP dispersions and polymer solutions. DLS also provides a measure for the hydrodynamic diameter $2R_H$ of individual nanocrystals (with R_H being the nanocrystal hydrodynamic radius), which accounts for subtle effects of surface ligand charges on the hydrodynamic interactions.[38] R_H is extracted from the autocorrelation function of the scattered signal and is often provided as a number or intensity distribution to account for size dispersity/ditsribution.[37,39] Figure 3C shows the experimental plots of the intensity versus hydrodynamic diameter for four representative TA-PEG-OCH_3−AuNPs dispersions prepared using different Au-to-ligand molar ratios. Single narrow peaks were measured for all four samples, indicating narrow size distributions in these dispersions (i.e., unimodal distributions and absence of aggregate formation; see Figure 3C). Table 1 shows the average values of the hydrodynamic diameter measured for these samples side-by-side with those extracted from TEM; only hydrodynamic diameters for the larger size are provided as weak scattering prevented the collection of reliable DLS data for smaller size NPs ($2R_{TEM} < 5$ nm). A ratio R_{TEM}/R_H of ~0.55 was measured for the various samples. The larger hydrodynamic sizes were consistently measured for the various dispersions due to contributions from the ligand shell (TA-PEG-OCH_3) and hydrodynamic interactions.[37−39] This confirms our previous DLS measurements applied to CdSe and CdSe-ZnS quantum dots, where the sizes extracted from DLS were also consistently larger than those derived from TEM; a ratio of 0.5 was measured for those materials.[39] The difference between R_{TEM} and R_H cannot be simply accounted for by a geometrical superposition of the metallic core plus the TA-PEG-OCH_3 ligands as discussed above.

DLS and TEM were combined to understand the effects of adding extra free ligands following complete growth of the nanocrystals (e.g., effects of extra passivation of the metal cores). TEM measurements showed that there were no differences between sizes measured for the as-prepared nanocrystals and for those subject to extra passivation. The intensity distribution data extracted from DLS showed single peaks, which indicates absence of potential etching or aggregation buildup after the addition of extra free ligands (Figure 3D). However, we consistently observed a small increase in the measured hydrodynamic size following extra passivation (compare data in Figure 3C and D); the increase was more pronounced for the larger size nanocrystals. For example, the hydrodynamic diameter increased from 21 nm for the sample prepared using a Au/ligand ratio of 2000:1 to ~25 nm for the same one following extra passivation (see Table 1). In comparison, the diameter measured by TEM was ~12 nm for both samples (Table 1). We infer from this change that addition of extra ligands essentially increases the density of the surface ligands on the nanocrystals (resulting in a more homogeneous surface coverage), which slightly changes the contribution of the hydrodynamic interactions to the measured size. The slightly larger increase in hydrodynamic diameter for larger size NPs (prepared using higher Au/ligand ratio) can be attributed to a lower ligand coverage of the nanocrystals during the initial growth. The ligand density is higher for their smaller size counterparts because higher molar concentrations of the ligands are used during the growth.

Colloidal Stability Tests. *1. Stability to Excess Salts, pH Changes, and Refluxing at Higher Temperature.* We first explored the effects of added excess NaCl on the colloidal stability of AuNPs[40] prepared using the various ligands introduced above, namely, TA-PEG-OCH_3 and TA (both are disulfide-terminated) along with HS-PEG-OCH_3 and MHA; the last three constitute control samples. For consistent comparison, we used similar size nanoparticles. Figure 4A shows side-by-side images of ~5 nm AuNPs grown using TA, HS-PEG-OCH_3, and TA-PEG-OCH_3 dispersed in deionized water with and without 2 M NaCl; data were collected after 30 min and 4 days of storage. We found that aggregation buildup combined with a clear color transformation took place for TA- and MHA-capped NPs (data for MHA−AuNPs are not shown); the dispersions changed color from red to violet immediately after salt addition and precipitated within 1 h. In comparison, dispersions of TA-PEG-OCH_3−AuNPs and HS-PEG-OCH_3−AuNPs were stable and aggregate-free

(40) Levy, R.; Thanh, N. T. K.; Doty, R. C.; Hussain, I.; Nichols, R. J.; Schiffrin, D. J.; Brust, M.; Fernig, D. G. *J. Am. Chem. Soc.* **2004**, *126*, 10076–10084.

(see Figure 4A); TA-PEG-OCH_3−AuNPs stayed dispersed and aggregate-free in 2 M NaCl solution at least for 8 months. Nonetheless, dispersions of HS-PEG-OCH_3−AuNPs became progressively unstable with time, and macroscopic precipitation was eventually observed after 1 month of storage at room temperature.

In the second stability test, we probed the effects of heating (refluxing at 100 °C) the nanocrystal dispersions for 30 min. The images shown in Figure 4B indicate that while TA−AuNPs changed color to dark purple, TA-PEG-OCH_3−AuNPs and HS-PEG-OCH_3−AuNPs were essentially unaffected, even though HS-PEG-OCH_3−AuNPs exhibited a slight change in color following heat treatment (see Figure 4B). Dispersions of MHA−AuNPs changed to colorless and precipitated (data not shown). The UV−vis absorption spectra recorded for TA-PEG-OCH_3−AuNP dispersions have identical SPB peaks before and after heat treatments (Supporting Information, Figure S3). Effects of heating were also tested in the presence of additional excess free ligands (30 min refluxing with additional TA-PEG-OCH_3, 10 times higher than Au atom in solution) and in the presence of Dulbecco's modified Eagle's growth medium. We found no change either in NP size (extracted from TEM) or in the absorbance spectra collected before and after heat treatment. In addition, the TA-PEG-OCH_3−AuNPs exhibited remarkable stability when dispersed in growth media with no change in the absorption spectra and no aggregate formation; further details are provided in the Supporting Information (Figures S3 and S4).

In the third test, we probed the effects of pH changes on the stability of nanocrystals prepared using the same set of ligands. The dispersion pH was controlled by adding a few drops of 2 M NaOH (basic) or HCl (acidic) solution to the NP dispersions. We found that dispersions of TA-PEG-OCH_3−AuNPs stayed stable (no color change) and aggregate-free over the pH range of 2−13 for at least 9 months (see Figure 4D). HS-PEG-OCH_3−AuNPs also stayed well dispersed at the same pH range, though there was a slight color change from reddish to bright pink at lower pH (Figure 4D). Dispersions of TA−AuNPs and MHA−AuNPs, in comparison, aggregated at pH ≤ 4 and pH ≤ 5, respectively, after 1 day of storage (see Figure 4D). We should stress that the stability of AuNPs synthesized using our one-phase growth method in the presence of TA-PEG-OCH_3 ligands was similar to that observed for AuNPs ligand-exchanged with TA-PEG-OCH_3 from citrate-stabilized nanocrystals.[33,35]

These results indicate that the colloidal stability of AuNP dispersions to added excess ions, changes in solution pH, and heat treatment was enhanced when the NP growth was carried out using PEGylated ligands. The terminal PEG promotes better affinity to the surrounding aqueous media by reducing interparticle attractions, which results in substantially enhanced steric stabilization of the NPs against added salts, changes in pH, and heat treatment. Importantly, the stability was further improved for NPs capped with disulfide-terminated ligands (TA-PEG-OCH_3) compared with single thiol-terminated ligands (MHA and HS-PEG-OCH_3).

2. Dithiothreitol Competition. Dithiothreitol (DTT) is a small molecule known to have high affinity to Au surfaces due to its dithiol function. Thus, stability test of TA-PEG-OCH_3−AuNPs against competition from DTT will be very informative, as it permits one to assess the ligand binding affinity to the nanocrystals. It also provides information on how AuNPs potentially behave in biological media which are often rich in sulfur containing biomolecules, such as cysteine and glutathione. DTT is one of the most abundant chemicals used for reducing disulfide bond of proteins, antibodies, and other disulfide containing biomolecules.[41,42] It can displace thiol-terminated ligands away from the NP surface, which potentially results in aggregate buildup with time. Ligand displacement by DTT alters the spectroscopic properties of the AuNPs, including a decrease in the SPB peak and change in the dispersion color, along with an increase in the absorbance at longer wavelengths. We compared the "resistance" of three sets of aqueous AuNP dispersions, capped with TA, HS-PEG-OCH_3, and TA-PEG-OCH_3 ligands against 0.5 M DTT at pH 8 (see Figure 4C). The three sets of NPs have ∼5 nm core size and were prepared using Au/ligand molar ratios of 100:1 (for TA-PEG-OCH_3), 15:1 (for HS-PEG-OCH_3), and 100:1 (for TA). The Au/ligand ratio varied from one set to another due to difference in the NP growth rate for each ligand. The absorption spectra measured for these samples had identical absorption features prior to addition of DTT (see Supporting Information, Figure S5). The data showed that TA-PEG-OCH_3−AuNPs were essentially unaffected by the presence of DTT. In comparison, TA−AuNPs experienced a slight color change to purple, while HS-PEG-OCH_3−AuNPs completely precipitated after 1 day of storage at room temperature (Figure 4C). This test is simple yet very informative, and it indicates that there is an added benefit to using surface ligands that have both the bidentate anchoring group and a PEG segment compared with those missing either module. The stronger resistance to competition from other thiol containing compounds can drastically enhance the colloidal stability in biological environments (often rich in sulfur containing proteins) and expand the opportunity for using these NPs in biological targeting and imaging.[32]

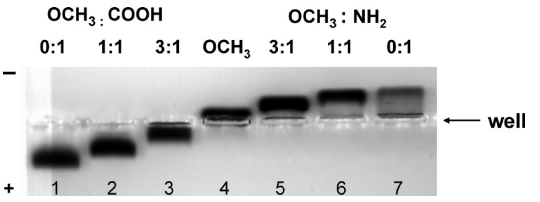

Figure 5. Gel electrophoresis of TA-PEG−AuNPs following extra passivation with mixed OCH_3- and COOH- or NH_2-terminated ligands; samples shown were treated with TA-PEG550-OCH_3/TA-PEG600-COOH = 0:1, 1:1, 3:1 (lanes 1−3), 100% TA-PEG550-OCH_3 (lane 4), and TA-PEG550-OCH_3/TA-PEG600-NH_2 = 3:1, 1:1, 0:1 (lanes 5−7).

The stability tests described here are very informative and very relevant to applications in biology. For example, assays based on DNA hybridization are often carried out under harsh conditions (such as high concentrations of salts and relatively high temperatures, ∼60 °C).

***In Situ* Surface-Functionalization of AuNPs.** One additional advantage offered by the present synthetic approach is the ability to control the surface functionalities of the AuNPs. This can be achieved by mixing end-functionalized TA-PEG ligands (e.g., carboxylic acid, amine, biotin, azide) together with the inert TA-PEG-OCH_3 ligands during the final passivation step. In this study, we used TA-PEG600-COOH or TA-PEG600-NH_2 in the mixture at different OCH_3/COOH (or NH_2) ratios (i.e., 0:1, 1:1, 3:1, 1:0). Figure 5 shows the gel electrophoresis image collected from 5 nm AuNPs prepared using the above mixing ratios; experiments were run on 1% agarose gel for 10 min at 7 V/cm. The gel image clearly shows that while AuNPs passivated with

(41) Agasti, S. S.; You, C. C.; Arumugam, P.; Rotello, V. M. *J. Mater. Chem.* **2008**, *18*, 70–73.

(42) Wiita, A. P.; Koti Ainavarapu, S. R.; Huang, H. H.; Fernandez, J. M. *Proceed. Nat. Acad. Sci.* **2006**, *103*, 7222–7227.

TA-PEG-OCH_3 (OCH_3/COOH = 1:0) did not exhibit any mobility shift under applied voltage, NPs functionalized with OCH_3/COOH and OCH_3/NH_2 mixtures experienced a sizable and ratio-dependent mobility shift. Furthermore, the sign of the mobility shift confirmed the presence of negative charges for carboxyl-terminated ligands (AuNPs migrated toward the anode) and positive charges for amine-terminated ligands (AuNPs migrated toward the cathode). This demonstration clearly indicates that our synthetic method can allow *in situ* functionalization of the AuNPs with an array of reactive end groups.

We would like to stress the fact that surface functionalization of the AuNPs with the desired reactive groups using our synthetic design is effective and simple to implement, because the mixed ligands used in the passivation step are essentially identical (the same anchoring groups and same PEG) and thus have the same affinity to the nanocrystal surfaces. Varying the fraction of the reactive ligands in the mixture would ultimately allow control over the number and type of reactive groups per NP. This concept has been tested, even though via cap exchange with the reduced form of the ligands (DHLA-PEG), with CdSe-ZnS quantum dots; nanocrystals have been separately functionalized with discrete fractions of amines and carboxylic acid groups.[33] A variety of other end groups could be used.

In situ functionalization with the desired terminal group can substantially simplify sample manipulation by avoiding additional ligand exchange step(s) often required with commercially available citrate-stabilized AuNPs.[33,40] It also facilitates controlled coupling to target molecules such as biological receptors (proteins, peptides, DNAs) and dyes. Further targeted biological studies using AuNPs that have been *in situ* functionalized with additional reactive groups are underway, including assay development intracellular uptake. Results will be presented in future reports.

Elucidation of Interactions between Aurate and Disulfide Groups: Precursor Formation. To gain additional insight into what may potentially initiate and affect the NP growth, we probed the interactions between TA-PEG-OCH_3 and Au ions by measuring changes in the UV−vis absorption properties of aurate-plus-ligand mixtures in the absence of $NaBH_4$ reducing agent. For comparison, we carried out similar experiments using mixtures of aurate with TA, DHLA-PEG-OCH_3, and HS-PEG-OCH_3 ligands. The time-trace curves of the absorption spectra collected from mixtures of TA-PEG-OCH_3 (and HS-PEG-OCH_3) with aurate are shown in Figure 6; additional spectra are provided in the Supporting Information (Figure S6). There are two distinct peaks at ~220 and ~290 nm for the pure aurate solutions (see Figure 6 and Supporting Information, Figure S6), which have been assigned to the presence of $AuCl_4^-$ ions.[43] Upon mixing with the ligands, one can isolate two distinct trends in the absorption spectra. In the presence of TA-PEG-OCH_3 the peaks at ~220 and 290 nm decreased with time, while an additional broad peak at 360 nm progressively built up; saturation was rapidly reached (within ~40 min; see Figure 6A). In the mixtures with HS-PEG-OCH_3, the decrease in the peak amplitudes at 220 and 290 nm was slower (saturation was reached after ~140 min), and there was no additional peak at 360 nm. With aurate/TA mixtures, the change in the absorption spectrum (namely, the peaks at 220 and 290 nm) were much smaller and rapidly reached saturation. Furthermore, there was no additional absorption peak at 360 nm as observed for TA-PEG-OCH_3 (see Supporting Information, Figure S6). In contrast, mixing aurate with DHLA-PEG-OCH_3 ligands produced a very rapid decrease in the peaks at ~220 and ~290 nm, and saturation was reached within 15 min. Furthermore, as with the HS-PEG-OCH_3, there is no new peak appearing at ~360 nm (see Supporting Information, Figure S6).

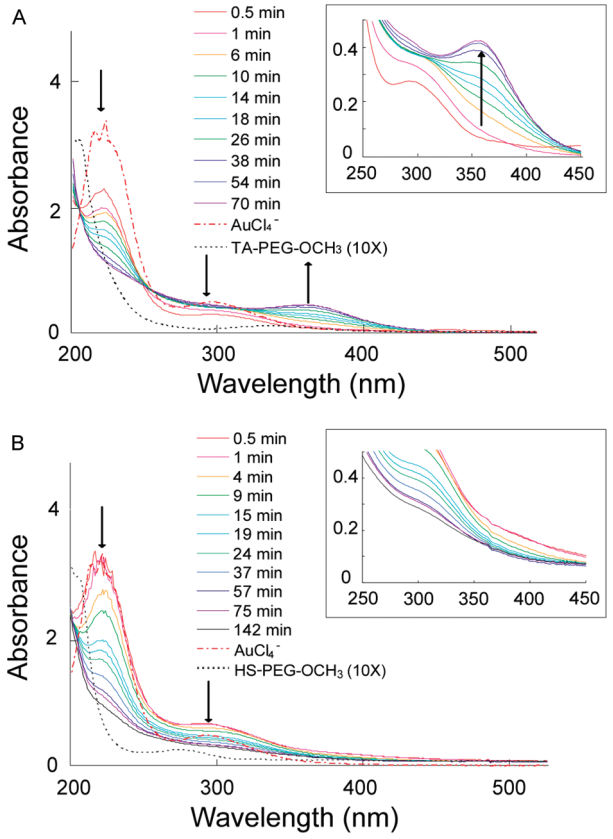

Figure 6. Time-dependent UV−vis absorption spectra for $HAuCl_4$ and ligand mixtures (Au/ligand = 3:1, concentration of ligand = 106 μM). (A) TA-PEG-OCH_3 and (B) HS-PEG-OCH_3. Changes in the spectra are indicative of ligand to gold complex (precursor) formation. The spectra for other ligands including TA and DHLA-PEG-OCH_3 are provided in the Supporting Information. Excess of 10× corresponding to 1.06 mM was used for the pure ligands.

We attribute the changes in the absorption features to transformation of $AuCl_4^-$ ions in the presence of the thiol or dithiolane containing ligands, where chlorides are replaced with "thiol(s)" or "disulfide" groups.[43] This Au-ligand precursor formation follows different "rates" for the various ligands used; rates are slow for HS-PEG-OCH_3, moderate for TA-PEG-OCH_3, and fast for DHLA-PEG-OCH_3. (We do not specify whether it is Au(III) or Au(II) that is involved in the precursor formation.) We assign the new peak at 360 nm to a progressive Au-TA-PEG-OCH_3 (specific for disulfide) precursor formation with time. Free disulfides (TA-PEG-OCH_3 alone) exhibit a very weak absorption peak at ~340 nm, but their contribution to the measured spectra is negligible at the concentrations used (106 μM) (see Figure 6A).[44] The different behavior observed with TA may be attributed to a rather poor solubility of the ligand in water (TA is usually dissolved in a small amount of methanol first before it is diluted in water), combined with a potential interference from the COOH group with complexation between $AuCl_4^-$ and TA. Finally, the data shown in Figure 6 also indicate that overall complexation between Au and ligand (i.e., formation of precursors) takes place prior to, and independent of, addition of the reducing agent.

(43) Torigoe, K.; Esumi, K. *J. Phys. Chem. B* **1999**, *103*, 2862–2866.

(44) Bucher, G.; Lu, C. Y.; Sander, W. *ChemPhysChem* **2005**, *6*, 2607–2618.

A close look at these results provides insight into an understanding of the different growth properties observed in our investigation: (1) The absence of a clear Au-TA complex for mixtures with TA leads to inconsistent growth, providing only a narrow size range. (2) With DHLA-PEG-OCH_3 ligand, the rapid formation of the Au-dithiol-PEG produces a strongly bound precursor, which may interfere with the Au reduction in the presence of $NaBH_4$; this would eventually produce a smaller size for comparable Au-to-ligand ratios. (3) Conversely, with HS-PEG-OCH_3, the Au-to-ligand binding in the complex is also strong, and this produces a narrower size range though the stability of the AuNPs is enhanced. (4) Finally, in the presence of TA-PEG-OCH_3, the issues associated with TA and the strong binding exhibited by DHLA-PEG-OCH_3 and HS-PEG-OCH_3 become less important. The slightly weaker interactions in the Au-TA-PEG-OCH_3 precursor allow controlled reduction of the Au ions and facilitate a more controlled NP growth, especially for the large size NPs prepared using large Au/ligand ratios. This produces growth of a more homogeneous nanocrystal population over a broader size range, which could not be achieved using the other ligand configurations. We should emphasize that $NaBH_4$ also initiates reduction of the disulfide end groups (because 10× excess of $NaBH_4$ was used),[33,34] which then produces dithiol-driven anchoring of the ligands with the AuNP surface; this strong anchoring produces enhanced colloidal stability of the resulting nanoparticles. The PEG tail provides an inert segment that reduces undesired interference with the precursor formation and further provides better affinity to the surrounding water phase. The dithiol-driven coordination combined with the presence of PEG on the ligand are at the origin of the better colloidal stability observed for TA-PEG-OCH_3−AuNPs in the presence of excess salts, changes in solution pH, and their resistance to competition by DTT.

Conclusion

We developed a water-based synthesis and growth method of a series of AuNPs using a modular bidentate PEG ligand. Our synthetic method relies on the use of modular ligands made of PEG appended with a disulfide anchoring group. The present approach allows us to control the nanocrystal size over the range between 1.5 and 18 nm which is a much wider size regime compared with previous reported methods using strong Au−S interaction. The nanocrystal size is simply controlled by varying the molar ratio of Au to the PEG ligand. TA-PEG-OCH_3−AuNPs showed dramatically enhanced colloidal stability over a wide range of pHs (from 2 to 13), under high salt concentrations, and against DTT competition/displacement. Such superior stability results from the combined effects: (1) hydrophilic nature of long PEG chain and (2) tight binding offered by the bidentate dithiol anchoring group on Au surfaces.

Our growth method also permits *in situ* functionalization of the AuNP surface with ligands presenting the desired end groups (such as amine, carboxylic acid, and biotin) to promote biocompatibility. These features combined with the remarkable colloidal stability of these nanocrystals open up new opportunities for use in biological applications. For example, coupling of the present AuNPs to specific peptides and other biological receptors could allow the development of assays that can be carried in harsh conditions (e.g., *in vivo*) where the remarkable stability offered by these materials could be very beneficial. Attaching cell penetrating peptides and proteins onto these NPs could allow guided delivery of such conjugates inside live cells where targeted photothermal therapy can be applied.[32]

Experimental Section

^{1}H NMR, UV−Vis Spectroscopy, and Transmission Electron Microscopy. The ligands used were characterized by ^{1}H NMR. The spectra were recorded on a Bruker SpectroSpin 400 MHz spectrometer. Chemical shifts for ^{1}H NMR spectra are reported relative to tetramethylsilane (TMS) signal in the deuterated solvent (TMS, $\delta = 0.00$ ppm). All J values are reported in hertz. Electronic absorption spectra were recorded using an HP 8453 diode array spectrophotometer (Agilent Technologies, Santa Clara, CA). The spectra were collected using quartz cuvettes (Spectro Cells) with 0.5 or 1 cm optical path length.

Structural characterization of the prepared AuNPs was carried out using a JEOL 2200-FX analytical high-resolution transmission electron microscope, with a 200 kV accelerating voltage. Samples for TEM were prepared by spreading a drop of the AuNP dispersion onto the holey carbon film on a fine mesh Cu grid (400 mesh) and letting it dry. Individual particle sizes were measured using Olympus measureIT; average sizes along with standard deviation were extracted from analysis of ∼100 nanoparticles on average.

Dynamic Light Scattering. DLS measurements were carried out using a CGS-3 goniometer system equipped with HeNe laser illumination at 633 nm and a single-photon counting avalanche photodiode for signal detection (Malvern Instruments, Southcorough, MA). The autocorrelation function was performed by using an ALV-5000/EPP photon correlator (ALV, Langen, Germany) and analyzed using Dispersion Technology software (DTS) (Malvern Instruments). All AuNP solutions were filtered through 0.2 or 0.45 μm syringe filters (Millipore). The sample temperature was maintained at 20 °C. For each sample, the autocorrelation function was the average of three runs of 10 s each, and then repeated at different scattering angles from 50° to 110°. Then contin analysis was applied to extract intensity versus hydrodynamic size profiles for the dispersions studied.

Gel Electrophoresis. Gel electrophoresis experiments were conducted using AuNPs functionalized with (i) pure TA-PEG-OCH_3, (ii) mixture of TA-PEG-OCH_3/TA-PEG-COOH, and (iii) mixture of TA-PEG-OCH_3/TA-PEG-NH_2. The nanocrystal dispersions were run on a 1% agarose gel using tris borate EDTA buffer (TBE, 100 mM Tris, 83 mM boric acid, 1 mM EDTA, pH 8.3). AuNP dispersions were prepared with ∼0.5−1 μM concentrations in a 10% glycerol TBE loading buffer prior to use. The experiments were conducted using a voltage of 7−8 V/cm, and the images were captured using the white light mode of a Kodak Gel Logic 2200 imaging system.

Synthesis of TA-PEG Series. TA-PEG550-OCH_3, TA-PEG-OCH_3, TA-PEG600-NH_2 and TA-PEG600-COOH were synthesized, purified, and characterized following the procedures detailed in our previous reports.[32−34]

Synthesis of MHA-PEG550-OCH_3(HS-PEG550-OCH_3). *A. Synthesis of 6-(acetylthio)hexanoic acid ($AcS(CH_2)_5COOH$).* To 5.00 g (2.56×10^{-2} mol) of 6-bromohexanoic acid in dimethylformamide (100 mL) was added potassium thioacetate (8.6 g, 7.5×10^{-2} mol) in one portion at ∼0 °C. The deep red mixture was stirred for 30 min at room temperature, diluted with CH_2Cl_2 (250 mL), and washed three times with water. The organic layer was dried over Na_2SO_4, and the solvent was evaporated. The yellow crude product was purified by vacuum distillation. TLC (CH_2Cl_2/MeOH = 10:1 v/v) $R_f \sim 0.57$. ^{1}H NMR (400 MHz, in $CDCl_3$): δ (ppm) 2.87 (t, 2H, $J = 7.2$ Hz), 2.36 (t, 2H, $J = 7.4$ Hz), 2.33 (s, 3H), 1.55−1.71 (4H), 1.38−1.46 (m, 2H).

B. Synthesis of AcS-PEG550-OCH_3 (acetyl-S-$(CH_2)_5$CONH-$(CH_2CH_2O)_n$-$CH_2CH_2OCH_3$, ATA-PEG550-OCH_3). Amounts of 5.5 g (∼1.0×10^{-2} mol) of CH_3O-PEG550-NH_2,[23] 0.53 g (2.6×10^{-3} mol) of 4-(dimethylamino)pyridine (DMAP), and 1.2 g (1.0×10^{-2} mol) of *N,N′*-dicyclohexylcarbodiimide (DCC) were added to 70 mL of CH_2Cl_2. An amount of 2.0 g (1.1×10^{-2} mol) of $AcS(CH_2)_5COOH$ dissolved in 20 mL of CH_2Cl_2

was added dropwise to the reaction mixture in an ice bath under N_2. Then the reaction mixture was gradually warmed up to room temperature and further stirred overnight. The mixture was filtered through Celite, and the precipitate was rinsed with CH_2Cl_2. After evaporating solvent, 1 M of HCl was slowly added to the residue. The aqueous mixture was washed three times with ether and saturated by $NaHCO_3$. The product was extracted with CH_2Cl_2 (three times). The combined organic layers were dried over Na_2SO_4 and evaporated. The residue was chromatographed on silica gel with 10:1(v/v) CH_2Cl_2/MeOH to collect the product. TLC (CH_2Cl_2/MeOH = 10:1 v/v) $R_f \sim 0.55$. ^{1}H NMR (400 MHz, in $CDCl_3$): δ (ppm) 6.14 (br s, 1H), 3.58−3.71 (m), 3.53−3.58 (m, 4H), 3.46 (t, 2H, $J = 5.2$ Hz), 3.38 (s, 3H), 2.86 (t, 2H, $J = 7.6$ Hz), 2.32 (s, 3H), 2.18 (t, 2H, $J = 7.2$ Hz), 1.54−1.71 (m, 4H), 1.38−1.46 (m, 2H).

C. Synthesis of HS-PEG550-OCH$_3$ (MHA-PEG550-OCH$_3$). An amount of 1.0 g (1.4×10^{-3} mol) of ATA-PEG550-OCH_3 (AcS-PEG550-OCH_3) was dissloved in 50 mL of MeOH and purged with N_2. A total of 0.055 g (1.4×10^{-3} mol) of NaOH in 6 mL of water was injected into the reaction, and the mixture was stirred overnight at room temperature under N_2. HCl (0.5 M) was added to the reaction mixture for neutralization. After evaporation of MeOH, the product was extracted with CH_2Cl_2 (three times). The combined organic layers were dried over Na_2SO_4, and the solvent was evaporated. TLC (CH_2Cl_2/MeOH = 10:1 v/v) $R_f \sim 0.5$. ^{1}H NMR (400 MHz, in $CDCl_3$): δ (ppm) 6.29 (br s, 1H), 3.58−3.71 (m), 3.53−3.57 (m, 4H), 3.46 (t, 2H, $J = 5.2$ Hz), 3.38 (s, 3H), 2.5−2.56 (dt, 2H), 2.19 (t, 2H, $J = 7.2$ Hz), 1.6−1.67 (m, 4H), 1.38−1.46 (m, 2H), 1.35 (t, 1H, $J = 7.8$ Hz).

Acknowledgment. The authors acknowledge NRL, Office of Naval Research (ONR), the Army Research Office for financial support. E.O. was supported by a fellowship from the Korea Research Foundation (D00089). Some of the data were collected using the HRTEM characterization facility provided at the Nanoscience Institute (NRL). We also thank Igor Medintz and Dorothy Farrell for assistance with some experimental details.

Supporting Information Available: UV−vis absorption spectra collected from dispersions of monothiol-PEG-OCH_3−AuNPs, TA-PEG-OCH_3−AuNPs before and after refluxing, DLS data; UV−vis time trace for ligand-plus-aurate mixtures collected for TA and DHLA-PEG ligands. This material is available free of charge via the Internet at http://pubs.acs.org.